# A Method for Calculating Axisymmetric Afterbody Flows

A.J. Peace*
*Aircraft Research Association Ltd, Bedford, England*

**A numerical method for calculating the flow around axisymmetric afterbodies with single or coaxial jets is presented. The solution technique used is based on the modification of an Euler method to include a representation of viscous effects on the afterbody surface and in the wake region. The development of the afterbody boundary layer and its continuation into the wake is predicted by an integral boundary-layer method used in inverse mode. The boundary-layer equations can thus be integrated through a region of separated flow. Jet entrainment due to turbulent mixing is modeled empirically. Results from the method and their comparison with experimental data are presented. The agreement obtained demonstrates that the method can be used in a civil or military design environment.**

## Nomenclature

$C_{D,\beta}$ = pressure drag coefficient
$C_p$ = pressure coefficient
$E$ = total energy per unit mass
$F, G, H$ = flux vectors
$H$ = total enthalpy
$\bar{H}, H_1$ = boundary-layer shape factors
$JPR$ = jet pressure ratio $= P_{0J}/p_\infty$
$k_{ent}, k'_{ent}$ = entrainment constants
$M$ = Mach number
$P_0$ = total pressure
$p$ = static pressure
$q_n, q_t$ = normal and tangential velocity, respectively
$r, s$ = radial and surface coordinates, respectively
$T_0$ = total temperature
$t$ = time variable
$u, v$ = axial and radial velocity, respectively
$w$ = vector of conserved variables
$z$ = axial coordinate
$\gamma$ = ratio of specific heats
$\delta$ = boundary-layer thickness
$\theta$ = azimuthal coordinate
$\rho$ = density
$\Sigma$ = source strength (shear layer)
$\Sigma_{ent}$ = entrainment source strength

*Subscripts*

$b$ = body value
$J$ = jet value
$i, j$ = cell center indices
$\infty$ = freestream value
1 = external flow value
2 = jet value

## I. Introduction

ONE of the most important areas in the study of propulsion installation aerodynamics is the problem of the interaction between propulsive jets and the external surfaces of the nozzles from which they issue. A large part of the aircraft total drag can come from these afterbody regions, and it is therefore becoming increasingly apparent that large reductions in drag can result from judicious afterbody design. The cost of experimental testing using powered propulsion units is extremely high, however, and this implies a role for computational techniques in the design process.

The flowfield of a jet emerging from a nozzle and interacting with the freestream is highly complex. The task of developing a theoretical method capable of modeling all the physical processes involved is a difficult one. To date, two main categories of solutions have been attempted. The first consists of those methods that split the flowfield up into separate regions, each of which is modeled by a different equation set. These regions are then patched together to form a global description of the flowfield. Examples of such methods, all of which assume the flow to be axisymmetric, are those of Hodges,[1] Wilmoth,[2] and Kuhn.[3] The second category addresses the Navier-Stokes equations and solves for the complete flowfield simultaneously. Deiwert et al.,[4] Peery and Forester[5] and Wagner,[6] for example, have developed methods of this type.

A survey of eighteen afterbody prediction methods was recently undertaken in an AGARD working group, WG08. A description of the methods used by the contributors, the test cases set, and the results submitted can be found in the documentation[7] of the working group. A more concise version is presented in Ref. 8.

In this paper, a new calculation method is described for predicting the flow around axisymmetric afterbodies. This method belongs to the class of methods that patch together solutions in different regions of the flow, and the solution technique is therefore compared with other methods of this class.[1-3] All the methods in Refs. 1-3 assume the external flow to be potential but, in reality, entropy gains due to shock waves can have a significant effect on the pressures on the external surface of the afterbody. Also, they all assume supersonic inflow conditions for the jet calculations and, in two cases,[1,3] the jet flow is assumed to be purely supersonic throughout. In the present method, a time-marching Euler method[9] is used to calculate both the external flow and the jet flow, and this gives a nominally exact description of the inviscid flow. This Euler method is modified to include a vortex sheet fitting algorithm. This is rather a novel feature, and the reasons for its use and its implementation are described in some detail in this paper.

In common with the methods of Refs. 1-3, an integral boundary-layer method[10] is used to calculate the external boundary layer. However, in the present method, the separa-

Received July 2, 1986; revision submitted Oct. 28, 1986.

*Project Supervisor, Aerodynamics Department.

tion point and separated region are captured automatically by employing a semi-inverse matching technique[11] between the boundary layer and the external flow. This is in contrast to approaches by which the separation point is predicted more empirically.[1,3] The phenomenon of entrainment, which results from turbulent mixing in the wake region, is modeled in part by a continuation of the integral boundary-layer method into the wake region and in part empirically, as in Ref. 1. In this respect, Wilmoth's method[2] is superior, as it solves the parabolic jet mixing equations using the method of Dash and Pergament[12] to predict the entrainment effect.

The geometry capabilities herein allow for axisymmetric afterbodies with either a single-stream jet or coaxial jet (fan + core flow). At present, the afterbody base is constrained to have zero thickness. The limitation of axisymmetry obviously means that important issues such as engine/wing interaction or emerging twin jets are not addressed. However, it is believed that a theoretical tool, even with this constraint, can have a significant impact on the afterbody design process.

Following a basic outline of the method in Sec. II, descriptions of the individual components of the calculation procedure are given in Secs. III–VII. Results are presented and discussed in Sec. VIII, and conclusions concerning the method are then drawn, together with suggested improvements.

## II. Outline of Method

The procedure used to calculate afterbody flows involves the modification of an inviscid method to provide a representation of viscous effects in the flowfield. These viscous effects are assumed to be confined to thin layers on the afterbody surface and in the wake region.

To demonstrate the basic principles involved, it is sufficient to consider a geometry with a single-stream jet. The flow is assumed to be axisymmetric and the afterbody base has zero thickness. A cross section of the flowfield showing the physical processes involved is shown in Fig. 1. For the inviscid method, the flow is effectively divided into two regions, the external region and the jet region. The streamline that separates these regions is tracked, the grid aligned with it, and a vortex sheet fitted.

In the real flow, a pair of boundary layers will form on each surface of the afterbody and merge in the wake region. Only the external boundary layer is described here because it has the largest effect on the flowfield. It is assumed to flow off the body and to form a wake, which sits on the jet boundary, as defined by the dividing streamline. The wake develops purely in the external flow environment and is affected by the jet only through its geometric pluming effect. However, this procedure does not allow for the turbulent mixing that occurs between the external flow and the higher total pressure jet flow. This effect is modeled in the method by a simple correlation.

Detailed descriptions of the individual flowfield methods and their coupling together are presented in the following sections.

## III. Inviscid Method

The inviscid method is based on the solution of the Euler equations. These are solved using the finite-volume scheme of Jameson et al.[9] For axisymmetric flow, the equations of motion in cylindrical polar coordinates $(z, r, \theta)$ can be written in nondimensional form as

$$\frac{\partial w}{\partial t}+\frac{\partial F}{\partial z}+\frac{\partial G}{\partial r}+H=0 \tag{1}$$

The vector of conserved variables and the corresponding flux vectors are given by

$$w=r\begin{bmatrix}\rho\\ \rho u\\ \rho v\\ \rho E\end{bmatrix},\ F=r\begin{bmatrix}\rho u\\ \rho u^2+p\\ \rho uv\\ \rho uH\end{bmatrix},\ G=r\begin{bmatrix}\rho v\\ \rho uv\\ \rho v^2+p\\ \rho vH\end{bmatrix},\ H=\begin{bmatrix}0\\ 0\\ -p\\ 0\end{bmatrix} \tag{2}$$

where $(u, v)$ are velocity components in the $(z, r)$ directions, $\rho$ is the density, $p$ the pressure, $E$ the total energy, and $H$ the total enthalpy. For a perfect gas,

$$E=\frac{p}{\rho(\gamma-1)}+\tfrac{1}{2}(u^2+v^2),\quad H=E+\frac{p}{\rho} \tag{3}$$

where $\gamma$ is the ratio of specific heats.

The finite-volume discretization of Eq. (1) and its solution on a computational grid by a time-stepping algorithm are described in detail in Ref. 9 and are not reproduced here. It is only noted that in the solution technique, Eq. (1) is augmented by the addition of dissipative terms, which are designed to capture shock waves without oscillations and to provide a background dissipation throughout the flowfield. Surface pressures are evaluated using the normal momentum relation first given by Rizzi.[13]

The boundary conditions to be specified are the freestream Mach number $M_\infty$, the total temperature ratio $T_{0j}/T_{0\infty}$, the jet pressure ratio $P_{0j}/p_\infty$, and the jet Mach number $M_j$ if it exceeds unity.

In the present application of the solution of the Euler equations to afterbody flows, it has been found necessary to fit the vortex sheet, or slip line, which emanates from the afterbody trailing edge. This is in contrast to the normal procedure in which the vortex sheet is captured as part of the flow solution. It was found during initial investigations that a capturing scheme resulted in excessive artificial dissipation, as calculated by the Euler algorithm, across the vortex sheet. This dissipation is much larger than is found in airfoil Euler calculations, for example, due to the large difference in velocity between the external flow and the higher total pressure jet region, and an artificial mixing effect results in the wake region. To incor-

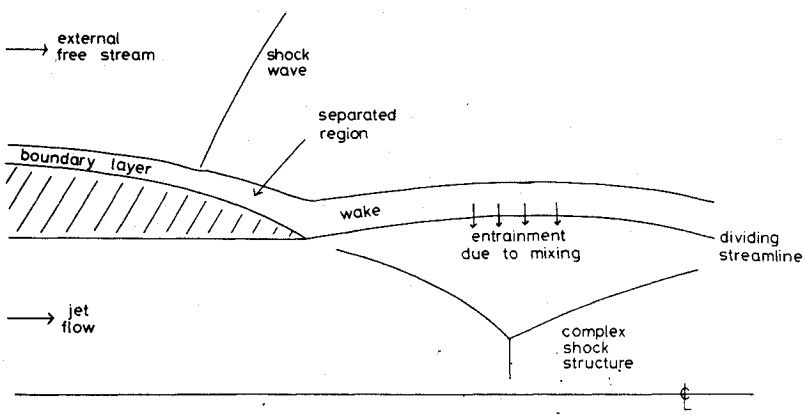


**Fig. 1 Schematic of afterbody flowfield.**

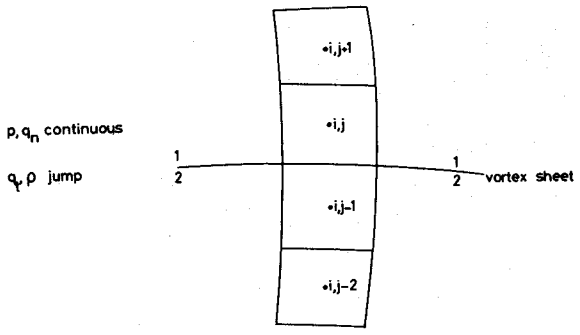


**Fig. 2 Vortex sheet fitting scheme.**

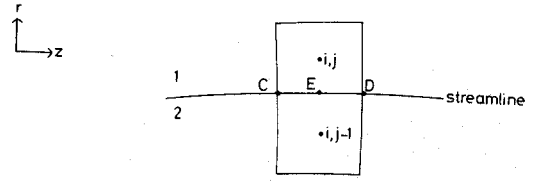


**Fig. 3 Streamline tracking algorithm.**

porate the effects of real entrainment in the flowfield model with this artificial effect being present is not feasible, and a vortex sheet fitting algorithm is therefore implemented, as is now described.

Consider a vortex sheet that is fixed in space. This discontinuity is a weak solution[14] of the Euler equations. This is a solution in which the normal velocity $q_n$ and pressure $p$ are continuous across the sheet, but the tangential velocity $q_t$ and density $\rho$ undergo discrete jumps. The continuity conditions ensure that the vortex sheet is a force-free stream surface.

Implementation of these conditions in the discrete model is as follows. Assume that the vortex sheet is aligned with a computational grid line. Then, with reference to Fig. 2, let values on either side of the sheet be denoted by subscripts 1 and 2. Also, let the finite-volume cells be labeled as indicated. Then the conditions applied on either side of the sheet are

$$\begin{aligned} \rho_1 &= \tfrac{1}{2}(3\rho_{i,j} - \rho_{i,j+1}) & \rho^2 &= \tfrac{1}{2}(3\rho_{i,j-1} - \rho_{i,j-2}) \\ q_{t1} &= \tfrac{1}{2}(3q_{t_{i,j}} - q_{t_{i,j+1}}) & q_{t2} &= \tfrac{1}{2}(3q_{t_{i,j-1}} - q_{t_{i,j-2}}) \\ q_{n1} &= \tfrac{1}{2}(3q_{n_{i,j-1}} - q_{n_{i,j-2}}) & q_{n2} &= \tfrac{1}{2}(3q_{n_{i,j}} - q_{n_{i,j+1}}) \\ p_1 &= \tfrac{1}{2}(p_{i,j} + p_{i,j-1}) & p_2 &= \tfrac{1}{2}(p_{i,j} + p_{i,j-1}) \end{aligned} \qquad (4)$$

It is also important to ensure that the dissipation terms are not differenced across the sheet. To reduce the truncation error and to facilitate the application of Eqs. (4), the grid used adapts itself so that the grid line that emanates from the trailing edge aligns itself with the vortex sheet. This technique is described in Sec. VI.

## IV. Shear Layer Calculation

The inviscid method as described in the previous section is modified to include a representation of viscous effects on the afterbody surface and in the wake. The shear layer that models these effects is calculated using the inverse form, as derived by East et al.,[10] of the original lag entrainment method of Green et al.[15] Details of this method and its solution in relation to the calculation of both attached and separated flows are given by Williams[11] and are not reproduced here.

The original derivation of the equations in the lag-entrainment method for axisymmetric flow is made under the assumption that the ratio of the boundary-layer thickness $\delta$ to the body radius $r_b$ is small. However, in the current application, the boundary-layer thickness can become very large and this ratio can approach unity. To remove this restriction, the modifications of the lag entrainment method due to Myring[16] are incorporated. These modifications require that the equations be written in terms of displacement and momentum areas rather than the usual displacement and momentum thicknesses. Although the form of the equations means that they are now valid for order-one values of $\delta/r_b$, the turbulence modeling as defined through the skin-friction and shape factor correlations remains unchanged. Thus, the modifications of the turbulence structure due to high flow curvature within the shear layer are not represented.

The boundary-layer equations require initial data to commence their integration. Only an initial momentum area and a value of the shape factor $\bar{H}$ need be supplied.

## V. Viscous/Inviscid Matching

The outer inviscid flow and the inner viscous flow, as described in the previous two sections, are matched together to form an equivalent inviscid flow. This equivalent inviscid flow is a representation of the real viscous flow as it would be calculated by the Navier-Stokes equations. A description of this concept is given by Lock and Firmin.[17]

The boundary conditions for the equivalent inviscid flow are obtained by the deficit formulation. In this approach, the Navier-Stokes equations are subtracted from the Euler equations, and the resulting expression is integrated across the shear layer. At the edge of the layer, the two equation sets are assumed equivalent. A composite expansion is then constructed for the Navier-Stokes variables in terms of the Euler and boundary-layer variables. Details are found in Johnston and Sockol.[18] The boundary conditions on the body surface and in the wake region are formed in terms of a source strength $\Sigma$ $(=q_n/q_t)$.

As explained by Williams,[11] the normal matching procedure, whereby the boundary-layer equations are integrated using a prescribed inviscid velocity gradient to obtain a displacement thickness, encounters a singularity at the separation point. To integrate past this point of vanishing skin friction, a semi-inverse matching procedure is used, whereby the source strength $\Sigma$ is treated as an independent variable of both the inviscid and viscous flow solutions.

To determine the means by which the source strength is updated, the results of a stability analysis, as described by Le Balleur[19] and Wigton and Holt[20] are used.

The final modification to be performed is to revise the normal momentum relation[13] in the Euler method to allow for nonzero normal velocity at the surface.

## VI. Grid Generation and Adaptation

The finite volume Euler scheme discussed in Sec. III is applied to a discretization of the flowfield into quadrilateral cells. In the generation of a computational grid that defines these cells, it is desirable to concentrate grid points in regions of high flow gradient. In the current problem of afterbody flows, these regions are near the solid surfaces and in the wake region where the jet interacts with the external flow. A stretched Cartesian grid is used to accomplish this point distribution.

To obtain a more accurate representation of the flowfield, the streamlines that emanate from the trailing edges of the geometry are tracked during the time integration of the Euler equations, and the grid is aligned with them; that is, a grid adaptation procedure is used.

Consider first inviscid flow, and assume that a steady-state solution has been reached. The grid is now aligned with the trailing-edge streamline that divides region 1 from region 2, as shown in Fig. 3. Then, from continuity of normal velocity

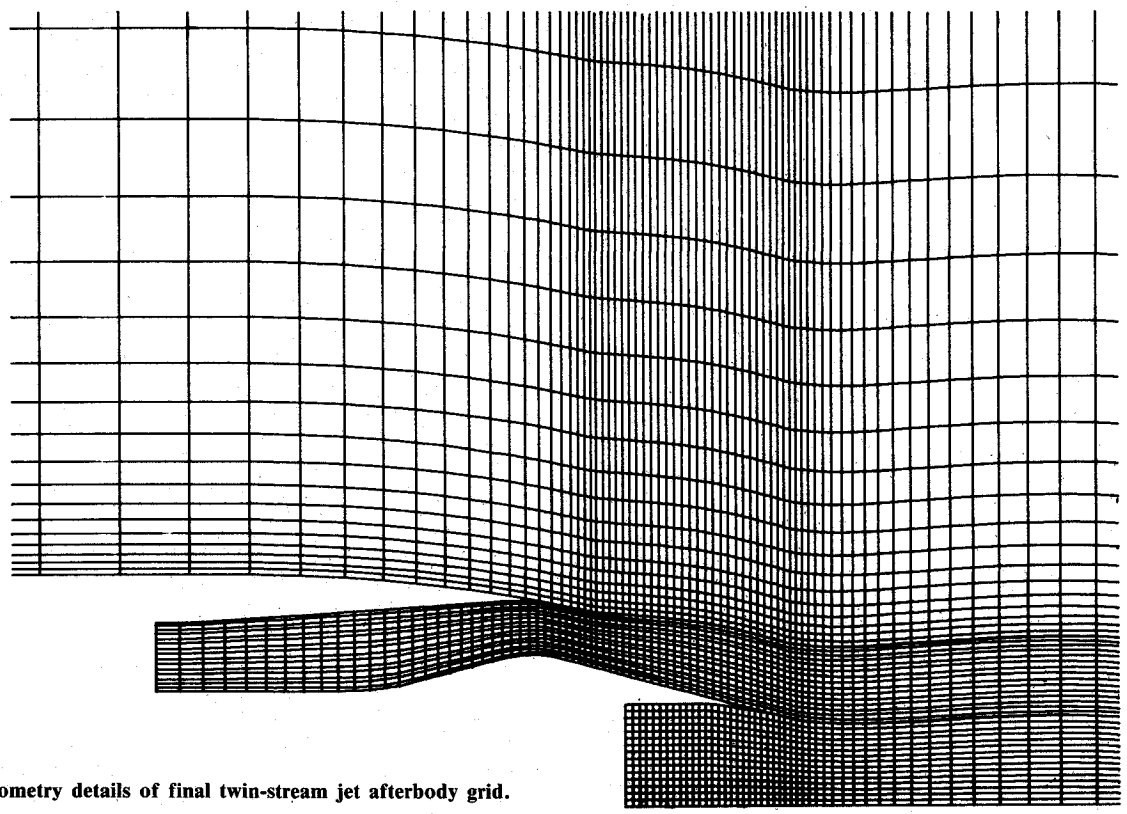

**Fig. 4 Geometry details of final twin-stream jet afterbody grid.**

across the dividing streamline, which also defines the vortex sheet position,

$$(q_n)_1 = (q_n)_2 = 0 \tag{5}$$

The latter equality can be rearranged to give

$$\frac{dr}{dz} = \frac{v_2}{u_2} \tag{6}$$

the equation of a streamline. If region 2 is associated with the jet region, this means that the dividing streamline can be tracked using flow velocities from the jet region only. The velocities are extrapolated from cell centers using a first-order formula, and Eq. (6) is integrated in the $z$ direction using (see Fig. 3)

$$r_D = r_c + (z_D - z_c) v_E / u_E \tag{7}$$

The grid moves during the transient behavior of the solution to align with the current position of the dividing streamline. When a steady state is reached, grid and streamline are coincident. An example of a grid from a converged solution is shown in Fig. 4.

Now, consider the case in which the inviscid boundary conditions are modified to create an equivalent inviscid flow that includes a representation of the viscous wake. Equation (5) is not used now because a jump in the normal velocity across the dividing streamline is used to model the wake. If the wake is calculated using flowfield variables from the external flow (region 1), i.e., it is the downstream development of the external boundary layer, then the streamline is still tracked using the jet values, Eq. (6). In fact, this streamline is now not strictly a streamline of the real flow but merely defines the boundary of the inviscid jet flow. This technique, however, does result in streamlines in the external flow that are a good approximation of the real flow. A representation of a shear layer on the jet-side surface of the geometry, and its development into the wake, can also be included in the method. The foregoing procedure is modified accordingly.

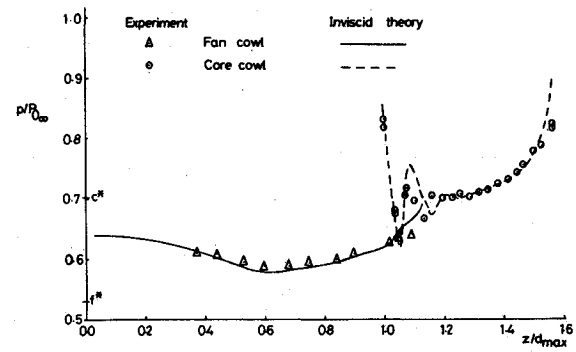


**Fig. 5 Results on coaxial jet afterbody for $M_\infty = 0.8$, $JPR_{FAN} = 2.02$, $JPR_{CORE} = 2.01$.**

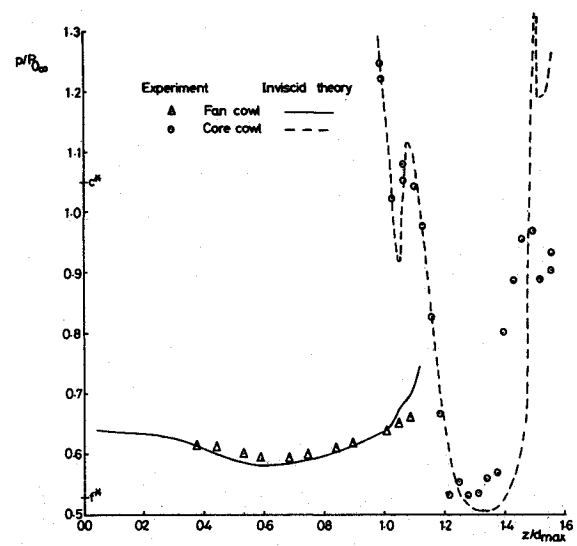


**Fig. 6 Geometry as Fig. 5. Results for $M_\infty = 0.8$, $JPR_{FAN} = 3.03$, $JPR_{CORE} = 3.01$.**

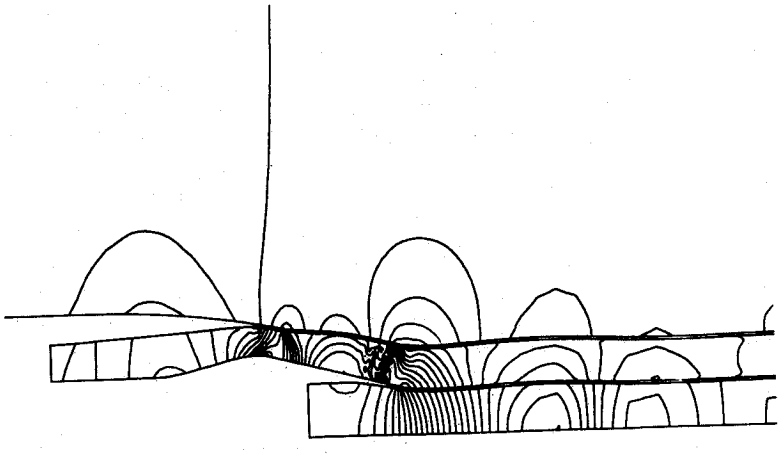

Fig. 7 Geometry as Fig. 5. Inviscid flow Mach number contours for $M_\infty = 0.8$, $JPR_{FAN} = 3.03$, $JPR_{CORE} = 3.01$.

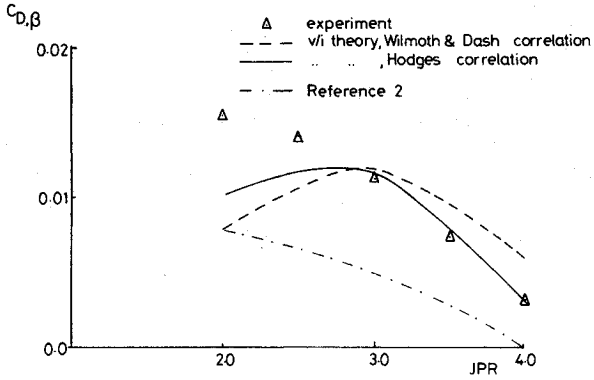


Fig. 8 Pressure drag coefficient against *JPR* for $M_\infty = 0.8$ on circular arc afterbody with 15 deg mean angle.

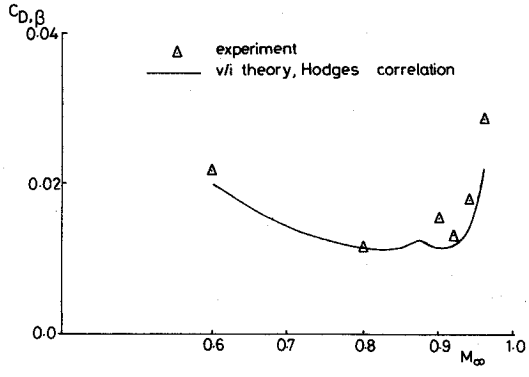


Fig. 9 Geometry as in Fig. 8. Pressure drag coefficient against $M_\infty$ for $JPR = 2.9$.

## VII. Entrainment Modeling

In the present application, the calculated shear layer described in Sec. IV develops purely in the external flow environment. The implication of this solution technique is that the turbulent mixing that takes place between the external and jet fluid is not modeled. This mixing causes an entrainment of fluid into the jet region. The effect of this phenomenon on, say, the afterbody surface pressures, cannot be neglected. Therefore, to attempt to model this entrainment and to improve flowfield predictions, a correlation is introduced into the method.

A similar correlation is applied in Hodges' method,[1] and in his work the entrainment source strength is given by

$$\Sigma_{ent} = k_{ent}[1 - (q_{t_2}/q_{t_1})] \tag{8}$$

where fluid is entrained from regions 1 to 2 and $k_{ent}$ is a constant of proportionality. Wilmoth and Dash[21] also proposed a correlation deduced from calculations they performed in which two coflowing streams were allowed to mix together. Their correlation can be written as

$$\Sigma_{ent} = k'_{ent}(q_{t_2}/q_{t_1})[1 - (\rho_2 q_{t_2}/\rho_1 q_{t_1})] \tag{9}$$

Each of these correlations is used in the present work and is implemented as an additional source strength, to add to the wake source strength, on the dividing streamline. The relative merits of these correlations are addressed in the following section.

## VIII. Results and Discussion

Results from the afterbody method described in the previous sections are now presented and compared with experimental data. These results fall into three classes: 1) inviscid solutions on a coaxial jet geometry, 2) viscous/inviscid solutions for attached flows on a single-stream jet geometry, and 3) viscous/inviscid solutions for separated flows on single-stream jet geometries. Both pressure distributions on the afterbody surfaces and flowfield contour plots are included. All cases below are run with the total temperature ratio set equal to unity, i.e., cold jets. This is done to provide a direct comparison with the experimental data and is not a limitation of the method. It is also noted that viscous-inviscid solutions on coaxial jet cases can also be obtained.

### Inviscid Solutions

The afterbody considered here is a research geometry with both a fan cowl and a core cowl, so that a coaxial jet was produced in the experimental tests. The tests were performed in the 9- × 8-ft transonic wind tunnel at ARA Ltd. This geometry is typical of that found on modern civil aircraft propulsion units. Figures 5 and 6 show two sets of inviscid theoretical pressures for jet pressure ratios ($JPR = P_{0j}/p_\infty$) of 2.0 and 3.0 at $M_\infty = 0.8$. Values of $p/P_{0\infty}$ for which $M = 1$ in the fan flow and the core flow are indicated on the axis by $f^*$ and $c^*$. Both cases show good agreement on the fan cowl. Although the flow is assumed to be inviscid, reasonable predictions of the fan cowl trailing-edge pressures are obtained. This is due to the zero included angles at the trailing edges, which allow the flow to pass over these points with nonzero velocities. If the angles were nonzero, the external flow would be predicted with a stagnation point at the trailing-edge upper surface. For the lower *JPR* case (Fig. 5), the fan flow is essentially subsonic, and results on the core cowl are in quantitative agreement. However, the fan jet flow contains a large supersonic pocket for the higher *JPR* case (Fig. 6), and only qualitative agreement is obtained on the core cowl. The flow characteristics of this latter case are easily visualized in the Mach number contour plot presented in Fig. 7. Note the

strong shock wave near the trailing edge of the core cowl. The contour discontinuities across the dividing streamlines, which coincide with the thick bands on the plot, are due to the differing total pressures in each region. (The bands are a function of the plotting routine only.) The grid shown in Fig. 4 corresponds to the converged solution in Fig. 7, and the grid lines clearly demonstrate the pluming in the fan flow around the supersonic bubble.

**Viscous-Inviscid Attached Solutions**

For this class of solutions, the afterbody considered is configuration 3 of the set tested by Reubush and Runckel;[22] the trailing-edge included angle is 15 deg. For this geometry, no separation was reported for all Mach numbers and *JPR*'s tested. The viscous-inviscid interaction scheme described in the previous section contains one free parameter, which has still to be specified.

The entrainment constant $k_{ent}$ (or $k'_{ent}$) must be tuned with available experimental data. Here, the data point $M_\infty = 0.8$ and $JPR = 2.9$ on configuration 3 was chosen, and the entrainment constant was fixed so as to reproduce the experimental pressure drag coefficient $C_{D,\beta}$. This gave a value of $k_{ent} = 0.074$ for the Hodges correlation, Eq. (8), and $k'_{ent} = 0.029$ for the Wilmoth and Dash correlation, Eq. (9).

Figure 8 shows a plot of pressure drag coefficient against *JPR* at $M_\infty = 0.8$ for each of the above correlations. The correlation due to Hodges can be seen to give the better comparison with experimental data. With this correlation, agreement for $JPR \geq 2.75$ is good but, for lower values of *JPR*, the difference between theory and experiment increases. The present predictions are also compared with those from Ref. 2. In Fig. 9, a plot of pressure drag coefficient against Mach number at $JPR = 2.9$ is presented using Hodges' correlation. Again, comparison with test data is good with a discrepancy arising for freestream Mach numbers approaching unity.

In fact, boattail drag is extremely sensitive to small changes in pressure distribution. Figure 10 illustrates the high level of agreement in afterbody pressure at a condition $M_\infty = 0.96$, $JPR = 2.03$. Examination of the other cases considered here showed a comparison of pressure apparently as good as in Fig. 10, even for the cases showing poorest agreement in Figs. 8 and 9. This is consistent with the conclusion of Ref. 8 that boattail drag is a poor assessment criterion for judging theoretical methods. However, it is the case that drag is perhaps the quantity of main interest to the designer. Comparison with the prediction of Ref. 2 in Fig. 10 demonstrates the superior shock representation of the present method.

A more valid criticism that could be leveled at the present method is that the value of $k_{ent}$ was calibrated at a data point of the experiments with which it is compared. However, picking up the trends observed here is not an automatic corollary of fixing one data point. Also, a similar level of agreement has

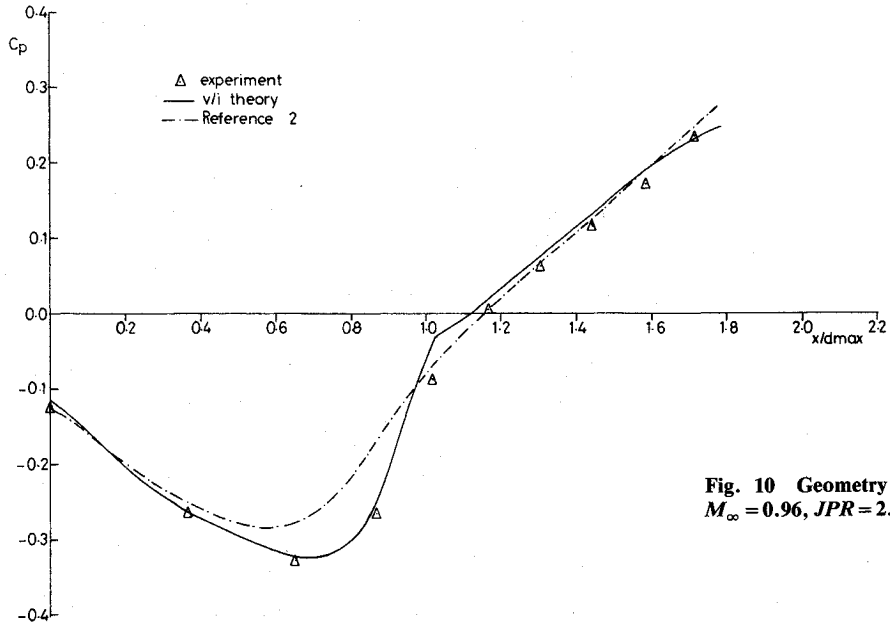


**Fig. 10 Geometry as in Fig. 8. Results on configuration 3 for $M_\infty = 0.96$, $JPR = 2.03$.**

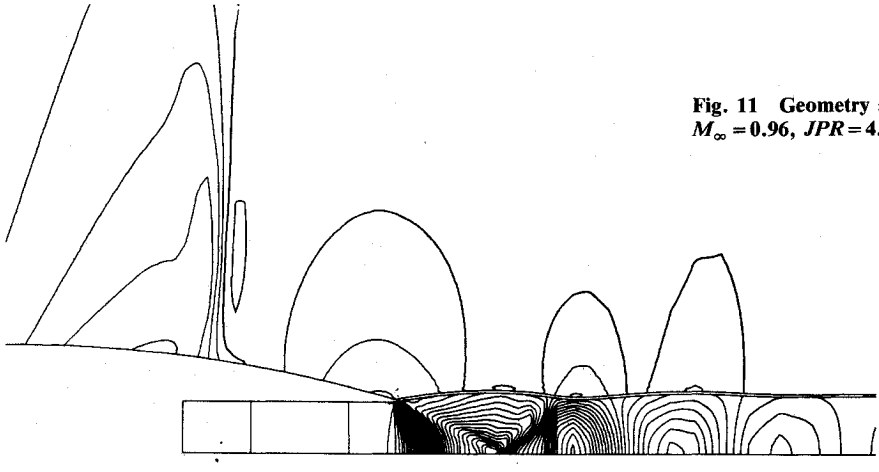

**Fig. 11 Geometry as Fig. 8. Viscous-inviscid pressure contours for $M_\infty = 0.96$, $JPR = 4.09$.**

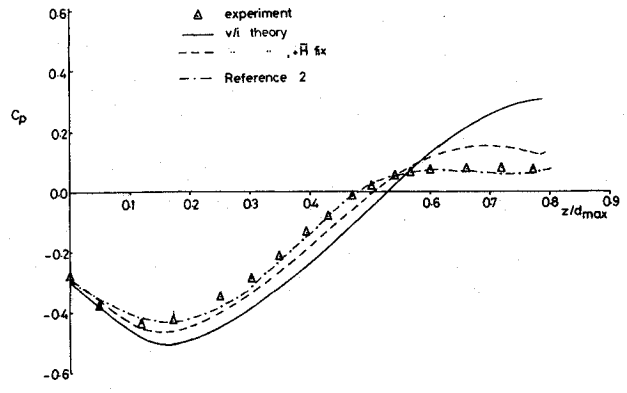


**Fig. 12 Results for $M_\infty = 0.8$, $JPR = 2.9$ on circular arc afterbody with 34 deg mean angle.**

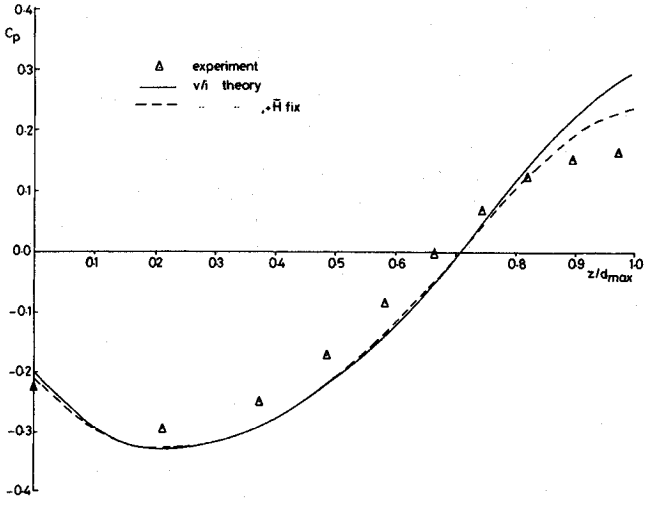


**Fig. 13 Results for $M_\infty = 0.7$, $JPR = 3.0$ on circular arc afterbody with 28 deg mean angle.**

been obtained for attached data in a different set of experiments[23] using the same value of $k_{ent}$ as that stated above.

A pressure contour plot for the condition $M_\infty = 0.96$, $JPR = 4.09$ is shown in Fig. 11. Continuity of pressure across the dividing streamline is observed, as forced by the Euler algorithm; the pluming of the jet and its internal cell structure are also clearly visible.

#### Viscous-Inviscid Separated Solutions

The use of the matching procedure described in Sec. V should allow regions of separated flow on the afterbody surface to be captured by the method. Configuration 1 in Ref. 22 has a trailing edge included angle of 34 deg and was the most severe geometry tested. All experimental data taken on this model are indicative of a large region of separated flow being present on the surface. However, both these data and the theoretical prediction from the method (continuous line) are shown in Fig. 12 for $M_\infty = 0.8$ and $JPR = 2.9$, and agreement is seen to be far from favorable. In fact, the development of the boundary layer as predicted by the method shows that the flow stays fully attached up to the trailing edge. The author believes that this is due to the shape factor relation used in the integral boundary-layer method being in error, for this class of flows, in the region of the favorable pressure gradient at the most forward part of the body. More precisely, the value of the shape factor $\bar{H}$ falls to a very low value ($\bar{H} = 1.1$), and this means that a small change in $\bar{H}$ results in a large change in the mass-flow shape parameter $H_1$, as dictated by this correlation (see Refs. 10, 11, and 15). This also results in other correlations in the boundary-layer method going outside their region

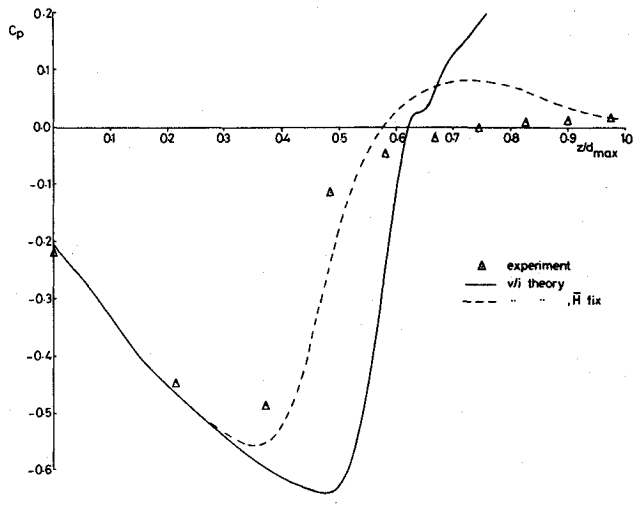


**Fig. 14 Geometry as Fig. 13. Results for $M_\infty = 0.94$, $JPR = 2.0$.**

of validity. Evidence to support this statement is presented in the form of the dashed line in Fig. 12. Here, a lower bound has been set on $\bar{H}$ ($\bar{H} \geq 1.25$) in the method to prevent the rapidly changing part of the shape factor correlation being reached. Separation of the flow is now predicted, and a much closer agreement with experiment is obtained. Further supportive evidence may be inferred from the unusually low value of $\bar{H}$ chosen in Hodges' method[1] to indicate a separation point. The same boundary-layer method is used in both Hodges' method and the present one. Obviously, the "fix" on $\bar{H}$ employed here is far from optimum. Nevertheless, it is retained for the the remainder of the comparisons shown in this section. The formulation of improved correlations for the type of flows considered here is no simple matter and is not considered further, except to note that the anomalous behavior in the boundary-layer method is present in the comparisons shown for attached flow but has a much smaller effect on the surface pressure distribution. The prediction of Ref. 2 shown in Fig. 12 is in excellent agreement with experiment, but in this calculation, the experimental separation position is input to the method, while in the present method, it is captured automatically.

To complete this section, two further examples of separated flow are shown in Figs. 13 and 14. These are on configuration 2 of Ref. 22. The trailing-edge included angle is 28 deg, and the conditions are $M_\infty = 0.7$, $JPR = 3.0$ and $M_\infty = 0.94$, $JPR = 2.0$. Results with and without the $\bar{H}$ modification show the measure of effect on the predicted pressures. With this modification, both cases show moderate agreement, although not of the standard achieved for the attached flow cases. The higher-speed case with the shock wave on the external surface in Fig. 14 is perhaps the more impressive comparison, suggesting that the method has a genuine capability of dealing with separated flow automatically, which could be improved further with a better approach than the lower bound on $\bar{H}$ set in the boundary-layer method. Also, the accuracy of the shape factor correlation in the boundary-layer method is questionable for large values of $\bar{H}$, and this may be responsible for the differences in pressure in the separated flow region. Similar conclusions were drawn in Ref. 24 in relation to airfoil calculations.

Computer times for the results in this section on a CRAY 1S machine are 33 $\mu$s/point/time step for a viscous-inviscid run. Generally, run times are about 500 s for a converged solution.

## IX. Conclusions

A numerical method for calculating the flow around axisymmetric afterbodies with single or coaxial jets has been presented. A vortex sheet fitting Euler algorithm has been

modified to include a representation of viscous effects. These viscous effects have been incorporated in part through an integral boundary-layer method and in part through an empirical correlation. By comparison of predictions from the method with experimental data, the following conclusions can be drawn: 1) Inviscid solutions provide good or reasonable agreement, depending on the complexity of the flowfield, if the trailing-edge included angle of the afterbody is zero. This has been demonstrated on a coaxial jet geometry, where good agreement is obtained for a nonchoked case and reasonable agreement for a choked case in which a strong shock wave develops on the geometry surface. 2) Viscous-inviscid solutions for attached flow cases are in excellent agreement with the experimental pressure distributions. Comparison with pressure drag coefficients shows that most of the trends are well predicted, but errors occur for small jet pressure ratios ($JPR < 2.5$). 3) Viscous-inviscid solutions for separated cases can give moderate agreement, provided that the correlations in the boundary-layer method are modified, albeit in a rather ad hoc way. 4) For choked jets, the method predicts the qualitative behavior of the jet structure, as seen through contour plots.

Finally, it is believed that the method, as described, can be of use to both civil and military aircraft designers. Future research is planned to increase its validity and to enhance its applicability. Improved entrainment modeling, better separated flow predictions, and increased geometrical complexity are possibilities. It is hoped that any modifications made will widen the overall use of the method.

## Acknowledgments

This work was carried out under contract to the United Kingdom Ministry of Defence (Procurement Executive).

## References

[1]Hodges, J., "A Method for Calculating Subsonic Flows over Axisymmetric Afterbodies Including Viscous and Jet Effects," RAE TR-82097, Oct. 1982.

[2]Wilmoth, R.G. "RAXJET: A Computer Program for Predicting Axisymmetric Flow over Nozzle Afterbodies with Supersonic Jet Exhaust," NASA TM-83235, Feb. 1982.

[3]Kuhn, G.D., "Calculation of Separated Turbulent Flows on Axisymmetric Afterbodies Including Exhaust Plume Effects," *AIAA Journal*, Vol. 18, March 1980, pp. 235–242.

[4]Deiwert, G.S., Andrews, A.E., and Nakahashi, K., "Theoretical Analysis of Aircraft Afterbody Flows," AIAA Paper 84-1524, June 1984.

[5]Peery, K.M. and Forester, C.K., "Numerical Simulation of Multistream Nozzle Flows," *AIAA Journal*, Vol. 18, Sept. 1980, pp. 1088–1093.

[6]Wagner, B., "Calculation of Turbulent Flow about Missile Afterbodies Containing an Exhaust Jet," AIAA Paper 84-1659, June 1984.

[7]"Report of the Working Group on Aerodynamics of Aircraft Afterbody," AGARD AR-226, June 1986.

[8]Putnam, L.E. and Bissinger, N.C., "Results of AGARD Assessment of Prediction Capabilities for Nozzle Afterbody Flows," AIAA Paper 85-1464, July 1985.

[9]Jameson, A., Schmidt, W., and Turkel, E., "Numerical Solutions of the Euler Equations by Finite Volume Methods Using Runge-Kutta Time Stepping Schemes," AIAA Paper 81-1259, June 1981.

[10]East, L.F., Smith, P.D., and Merryman, P.J., "Prediction of the Development of Separated Turbulent Boundary Layers by the Lag-Entrainment Method," RAE TR-77046, March 1977.

[11]Williams, B.R., "The Prediction of Separated Flow Using a Viscous/Inviscid Interaction Method," *Aeronautical Journal*, Vol. 89, May 1985, pp. 185–197.

[12]Dash, S.M. and Pergament, H.S., "A Computational Model for the Prediction of Jet Entrainment in the Vicinity of Nozzle Boattails (The BOAT Code)," NASA CR-3075, Dec. 1978.

[13]Rizzi, A., "Numerical Implementation of Solid Body Boundary Conditions for the Euler Equations," *Zeitschrift fürangewandte Mathewatik und Mechanik*, Vol. 58, 1978, pp. 301–303.

[14]Lax, P.D., "Weak Solutions of Nonlinear Hyperbolic Equations and Their Numerical Computation," *Communications on Pure and Applied Mathematics*, Vol. 7, 1954.

[15]Green, J.E., Weeks, D.J., and Brooman, J.W.F., "Prediction of Turbulent Boundary Layers and Wakes in Compressible Flow by a Lag-Entrainment Method," RAE TR-72231, Jan. 1973.

[16]Myring, D.F., "The Profile Drag of Bodies of Revolution in Subsonic Axisymmetric Flow," RAE TR-72234, May 1973.

[17]Lock, R.C. and Firmin, M.C.P., "Survey of Techniques for Estimating Viscous Effects in External Aerodynamics," *Proceedings of IMA Conference on Numerical Methods in Aeronautical Fluid Dynamics*, edited by P. Roe, Academic Press, Orlando, FL, 1983.

[18]Johnston, W. and Sockol, P., "Matching Procedure for Viscous-Inviscid Interactive Calculations," *AIAA Journal*, Vol. 17, June 1979, pp. 661–663.

[19]Le Balleur, J.C., "Strong Matching Method for Computing Transonic Viscous Flows Including Wakes and Separation," La Recherche Aérospatiale, No. 1981-3, 1981, p. 21.

[20]Wigton, L.B. and Holt, M., "Viscous-Inviscid Interaction in Transonic Flow," AIAA Paper 81-1003, June 1981.

[21]Wilmoth, R.G. and Dash, S.M., "A Viscous-Inviscid Interaction Model of Jet Entrainment," *AGARD Conference on Computation of Viscous-Inviscid Interactions*, AGARD CP-291, Oct. 1980.

[22]Reubush, D.E. and Runckel, J.F., "Effect of Fineness Ratio on Boattail Drag of Circular-Arc Afterbodies Having Closure Ratios of 0.50 with Jet Exhaust at Mach Numbers up to 1.3," NASA TN D-7192, May 1973.

[23]Reid, J. and Kurn, A.G., "The Effect of Boundary Layer Thickness on Afterbody Drag," RAE TR-79083, July 1979.

[24]Melnik, R.E. and Brook, J.W., "The Computation of Viscous/Inviscid Interaction on Airfoils with Separated Flow," *Third Symposium on Numerical and Physical Aspects of Aerodynamic Flows*, California State Univ., Long Beach, CA, 1985.